Effects of Ag or Si on precipitation in the alloy Al-2.5% Cu-1.5% Mg

Anne-Marie Zahra, Christian Zahra, Myriam Dumont

Effects of Ag or Si on precipitation in the alloy Al-2.5% Cu-1.5% Mg

Effects of Ag or Si on precipitation in the alloy Al-2.5 % Cu-1.5 % Mg

A.-M. ZAHRA, C.Y. ZAHRA and M. DUMONT [+]
Université Paul Cézanne – Aix-Marseille III
Thermodynamique, propriétés Electriques, Contraintes et Structures aux Echelles
Nanométriques (TECSEN), UMR 6122, CNRS,
Faculté des Sciences et Techniques de St. Jérôme,
Case 261, 13397 Marseille cedex 20, France

[+] Corresponding author. Email: myriam.dumont@univ.u-3mrs.fr

ABSTRACT

Calorimetric measurements and electron microscopy observations were performed on Al-2.5 mass% Cu-1.5 mass% Mg alloys containing also 0.4, 1 or 2 % Ag or 0.5 % Si, in order to improve understanding of the relationships between precipitation processes and age hardening. The analogous behaviour of calorimetric and hardness data confirms that the first hardening stage is initiated in all alloys by GPB zone formation which occurs via a nucleation and growth controlled mechanism. The vacancy-trapping effect of Mg is increased by Ag and Si additions and leads to slower precipitation kinetics. Consequently refined GPB zones sizes are obtained leading to an increase in hardness with respect to the ternary alloy. During the second hardening stage, the formation of the more stable S′ phase increases the total amount of strengthening precipitates in the ternary alloy. Phases typical for binary Al-Cu alloys form additionally in the Si-containing alloy. In the Ag-bearing alloys, precipitation of the hardening X′ phase occurs the earlier the higher the Ag content is; it is followed by S′ precipitation. During heating of the ternary alloy, the S′ phase forms after substantial dissolution of GPB zones and of the S″ phase identified by high resolution electron microscopy; this contradicts the concept of a continuous precipitation sequence.

Key words: aluminium alloys, age-hardening, calorimetry, clusters, GPB zones

1. Introduction

The precipitation processes in Al-Cu-Mg alloys which fall within the (α + S) region of the ternary phase diagram [1] have been the subject of numerous research due to their fundamental and commercial interest since the discovery of the alloy duralumin in

1906. Since then they have been studied mainly by mechanical testing, calorimetric measurements and electron microscopy observations. Two hardness stages are observable during ageing at medium temperatures [2,3]; a rapid initial rise which may account for 50 to 70 % of the total hardness increase, and a second rise, much slower than the first one. In semi-logarithmic representation, they are separated by a sort of plateau whose duration depends strongly on temperature and alloy composition. In normal scale, a plateau does not always appear [4].

More recently, atom probe field ion microscopy (APFIM), positron annihilation spectroscopy (PAS) and high resolution transmission electron microscopy (HRTEM) were applied to the study of these alloys; some of the results obtained with these new techniques are in contradiction with conclusions of earlier work.

a - The first controversy concerns the state of the solid solution (SS). X-ray and thermodynamic data indicate a clustering tendency between the Cu atoms in Al-Cu [5] and the Mg atoms in Al-Mg alloys [6] as well as a strong interaction between the Cu and Mg atoms in ternary alloys (e.g. [7]). However, it was concluded from three-dimensional atom probe (3D-AP) analyses on an Al-2.5 mass% Cu-1.5 mass% Mg alloy [8] that the solute atoms are still uniformly distributed after 1 min hold at 150 or 200 °C. Computer simulations of the decomposition process in these alloys also start from random atomic configurations in SS [9].

b - Disagreement also exists to explain the rapid decomposition after quenching leading to the first hardening stage. It is attributed either to the formation of Guinier-Preston-Bagaryatsky (GPB) zones (e.g. [3, 10-12]) or to solute atom clustering [13-16] or to solute atom-dislocation interactions [8] or to the presence of dislocation loops resulting from quenched-in vacancies [17]. The formation of GPB zones during ageing at temperatures as low as room temperature (RT) was deduced from X-ray [10],

hardness [18] and calorimetric [19,20] measurements but remains undetected by HRTEM due to their extremely small sizes (around 1 nm), hence is not accepted universally. The zones are considered to be cylindrical [10], mono- [20] or multilayered [21]. Besides, three-dimensional clusters visible by HRTEM after ageing at medium temperatures (e.g. 500h at 150°C) are designated by some authors as GPB zones [14,15]; energy dispersive X-ray spectroscopy (EDS) analyses performed on an Al-2.5% Cu-1.5% Mg-0.1% Si alloy (Mg:Cu atomic ratio of 1.5) and aged for 14 h at 200°C, show clusters enriched in Mg but not in Cu with respect to the matrix [22]. Hence they might correspond to the Mg-rich clusters observed by Charaï *et al.* [20] in a ternary alloy of similar ratio aged for 4 h at 200 °C. Clusters which are in most cases richer in Cu than in Mg, were found at 150 °C for Mg:Cu ratios of 0.4 and 1 [23]. All these clusters are characterised by a very high Al content of about 90% [23-25] and contain vacancies. Cu-Mg clusters detected by APFIM are considered to act as nucleation sites for GPB zones which precipitate only during the second stage of hardening [13,15,26].

c - The existence of a coherent S″ phase (or GPBII), analogous to θ″ (or GPII) in Al-Cu alloys, is also highly discussed. Recent simulations of Wang and Starink [27] based on an orthorhombic structure of composition $Al_{10}Cu_{3+x}Mg_{3-x}$ ($0 \leq x \leq 1$) match the electron microscopy image and diffraction pattern of Charaï *et al.* [20]. According to Shih *et al.* [28], S″ is identical to partially ordered GPB zones; according to Ringer *et al.* [26], S″ is a variant of S.

d - There is no unanimity whether the orthorhombic metastable S′ phase should be distinguished from the orthorhombic stable S phase (Al_2CuMg) or not [13]. The metastable character of S′ is linked to Cu:Mg ratios different from unity. Charaï *et al.* [20] observed slight differences between S′ and S in calorimetric and HRTEM studies

and proposed that, during the gradual evolution from S′ to S, the lattice parameters of S′ vary with size (degree of coherency) until they reach the values for the stable phase S which is non-coherent with the matrix. Nucleation of S′ is fairly independent of GPB zones (e.g. [29,13]) but is proposed to start from clusters [30] dominantly rich in Mg, if the alloy has a Mg:Cu ratio of 1.6 [20]. This is seemingly supported by HRTEM studies [31,22], although clusters are considered to be GPB zones on which S (or S′) particles may nucleate. Based on HRTEM, Radmilovic *et al.* [32] recently proposed a new model for the crystalline structure of the incoherent S phase which was criticised for energetic reasons [33].

e - The precipitation sequence operative in $(\alpha + S)$ alloys remains uncertain. The following one is most often cited [34] for decomposition from the supersaturated solid solution (SSSS):

$$\text{SSSS} \rightarrow \text{GPB zones} \rightarrow \text{S}'' \rightarrow \text{S}' \rightarrow \text{S}.$$

A shorter one is derived from ageing studies at 150 °C [13] :

$$\text{SSSS} \rightarrow \text{Cu-Mg clusters} \rightarrow \text{GPB zones} + \text{S} \rightarrow \text{S}.$$

A two-stage sequence was introduced by Charaï *et al.* [20] for alloys with Mg:Cu ratios around 1.6 :

$$\text{SSSS} \rightarrow \text{Cu-rich clusters} \rightarrow \text{GPB zones} \rightarrow \text{S}'' \rightarrow \text{quasi-complete reversion}$$

$$\text{SSSS} \rightarrow \text{Mg-rich clusters} + \text{Cu atoms from matrix and dissolving S}'' \rightarrow \text{S}' \rightarrow \text{S}$$

In agreement with APFIM studies (e.g. [26]), GPB zones are considered to nucleate from Cu-rich clusters and may transform into S″; only after substantial but not complete dissolution of S″, solute atoms may combine with residual clusters enriched in Mg and form the S′ phase which gradually approaches the composition Al_2CuMg by decreasing the solubility of Cu and Mg in Al towards their equilibrium values. Hence the fraction precipitated increases and may induce a new (second) hardness rise [11].

The precipitation kinetics of GPB zones and S′ are slowed down by increasing the concentration in Mg atoms which trap vacancies preferentially and hinder the diffusion of Cu atoms [3,12].

f - The influence of small Ag or Si additions to Al-Cu-Mg alloys was already examined several times but results are contradictory. GPB zone formation is mostly reported to be slowed down [3,18,22,35,36], whereas it is expected to be accelerated according to computer calculations [9]. At medium temperatures, a new and probably initially coherent phase, X′, appears in Ag-containing alloys [37]. This phase nucleates on sites of Mg-Ag co-clusters, forms hexagonal platelets on {111} matrix planes and approximates the composition of S with up to 5 at% Ag [15]. In Si-bearing alloys, S′ formation is found to be either enhanced [38] or retarded [35,36].

The aim of the present work is to resolve as many discrepancies as possible by carrying out calorimetric measurements and some phase characterizations by HRTEM on the same alloys as those used in many previous investigations [3,13-15,18,22,26,37,39,40] and by referring to existing hardness data and electron microscopy observations. Calorimetry is of special interest for studies involving nanometer sized precipitates which are difficult (and in many cases still impossible) to detect by direct methods. Moreover, heat flow calorimetry enables to measure the kinetics of a process over several days (weeks) and informs on the reaction mechanism.

2. Experimental

Five alloys were investigated in the shape of 1 mm thick specimens; their compositions (except for alloy 5 used by Hutchinson and Ringer [22]) were determined by inductively coupled plasma atomic absorption spectroscopy and are given in Table 1 in mass and atomic %; the uncertainty is estimated to ±0.1% for Cu and Mg. All these alloys were

solutionised for 1h at 500°C, quenched into water at RT and analysed in this state or aged beforehand at temperatures between RT and 200 °C for specified times. The Ag concentration in alloy 4 is still soluble at 500°C, as can be concluded from the mechanical properties [18] and DSC studies (present work) of alloys containing up to 2% Ag. In fact, hardness increases steadily with Ag content and surpasses the ternary alloy [18]. DSC runs show that even during heating at 20 K min^{-1}, complete redissolution of the precipitates is achieved at 500 °C except in the alloy with the highest Ag content in which some concentration inhomogeneities persist up to 530 °C (see figure 3).

Table 1 : Alloy compositions in mass % (at.%)

	Cu	Mg	Ag	Si
Alloy 1	2.5 (1.1)	1.5 (1.7)	<0.001	<0.01
Alloy 2	2.5	1.5	0.4 (0.1)	<0.01
Alloy 3	2.5	1.5	1.0 (0.25)	<0.01
Alloy 4	2.5	1.5	2.0 (0.5)	<0.01
Alloy 5	2.5	1.5	<0.001	≈0.5

Fe : 0.03	Zn < 0.005	Zr < 0.005
Mn < 0.01	Cr < 0.005	Sr < 0.001
Ni < 0.01	Ti < 0.005	Al balance

Isothermal calorimetric measurements were carried out at 30, 150 and 180°C with the help of Tian-Calvet heat conduction calorimeters measuring the heat flow, dH/dt, versus time. Hence these calorimetric curves give directly the isothermal reaction kinetics. Curves which display a heat flow minimum are typical for reactions involving nucleation and growth mechanisms and yield sigmoid-shaped curves when plotting the heat evolved (obtained by integrating heat flows) or the fraction transformed (e.g. [41].)

Twenty specimens of each alloy, 1 mm thick and 15 mm in diameter, are used to perform isothermal calorimetry experiments. The time elapsed between quenching of the specimens, drying and transfer into the calorimeter after preheating to a temperature slightly higher than that of the apparatus is about 5 min. As the parasitic heat effects due to the introduction into the calorimeter last for about 30 min in spite of preheating, curves are not quantitative for times < 30 min, but their relative importance is respected when assuring identical conditions for introduction (which are chosen in such a way that introduction of pure Al specimens of the same mass gives exothermic effects; see figure 1). Specimens were examined either directly after quenching or after pre-ageing at RT in order to assess the influence of pre-ageing on the precipitation kinetics of more stable phases.

Differential scanning calorimetry (DSC) was performed with a power-compensated thermal analyser (Perkin-Elmer DSC7) which measures heat flows as a function of temperature. All experiments were done at a heating rate of 20 Kmin^{-1} for which corrections for thermal inertia are small [42] and were neglected. In general, each experiment was repeated twice on quenched as well as on aged alloys. Base line corrections for drift which increases with temperature were done with the help of polynomial equations. The first 3 min are lost due to operation and temperature stabilisation of the specimen.

Thin foils for the electron microscopy studies were prepared by twin jet electropolishing at 250 K using a mixture of 33% nitric acid and 67% methanol. They were examined in a Jeol 2010 F, UPR 22 microscope having a spatial resolution of 0.19 nm. This instrument is located at the Centre Pluridisciplinaire de Microscopie électronique et de Microanalyse of the Faculty of Science.

3. Results and interpretation

3.1. Isothermal studies

3.1.1. Ageing at 30 °C. When isothermally aged at 30 °C (figure 1), all alloys show a heat flow minimum which is situated at about 0.5 h for alloy 1 (not visible at the scale chosen), 1.7 h for alloy 5, 3 h for alloy 2 and 11 h for alloy 3. Due to uncertain extrapolation to zero time, the respective heats cannot be distinguished but lie all within $-(13.5 \pm 1.5)$ J/g when integrating between 30 min and 4 days (d). These relatively high values are characteristic for the formation of a metastable/stable phase, presumably GPB zones, via a nucleation and growth process [41].

[Insert fig. 1]

3.1.2. Ageing at 150 and 180 °C. When aged at 150 °C (the corresponding curves are not reproduced), alloys 1 and 5 show an overlap of two exothermic reactions, a strong one which decays over the first day and a much weaker and slower one which forms a flat minimum after several days and was attributed to S′ formation [20]. It is attained around 9.5 days in alloy 1 but is still not reached after 14 days of experiment for alloy 5. Only falling heat flows corresponding to growth processes are recorded for alloys 2 and 3.

[Insert fig. 2]

Curves obtained at 180 °C, given in figure 2, show a more rapid kinetic evolution than at 150 °C. It is proposed that after partial GPB zone dissolution (initial endothermic effects which last longer in pre-aged samples), the main exothermic peak in alloy 1 (curve 1) represents S′ formation via a nucleation and growth controlled mechanism and its gradual transformation into S. As its heat value, $-(12.5\pm1)$ Jg^{-1}, is lower than the value obtained by DSC (§3.2.), it has to be concluded that another phase,

probably S″ formed from GPB zones, dissolves simultaneously at longer ageing times. In fact, the presence of the S″ and S′ phases after 15 h ageing at 180 °C was confirmed by electron microscopy (§3.3) and DSC (curve similar to the one obtained after 4 h at 200 °C in figure 7(a)). Precipitation of the S′ phase in a similar alloy aged at 190 °C has also been observed by TEM [35]. S′ precipitation is reinforced by pre-ageing at RT (curve 1a) and, to a lesser extent, at 100 °C (curve 1b). However, no changes in the heat value or in the time position of the maximum rate of transformation are observed as compared to the water quenched sample. This suggests that pre-ageing influences the nucleation process by changing the number of nuclei and/or defects (dislocation loops and helices) but not the rate of S′ growth via Cu atom diffusion. The shape and relative position of the curves 1a and 1b exclude important direct transition of bigger GPB zones and/or S″ particles into S′ avoiding nucleation problems.

The Si addition in alloy 5 induces a slower rate of the major precipitation process at 180 °C (figure 2, curve 5) as compared to alloy 1. The asymmetry of the peak indicates the presence of two overlapping subpeaks; they are ascribed to θ′ and S′ formation, as the alloy composition is close to the (α + S + θ) field [22]. Pre-ageing at low temperatures (curve 5a) has a retarding effect on precipitation; DSC measurements performed on specimens aged for 1 d at 180 °C with and without 7 d hold at RT confirm that the overall precipitation is indeed less advanced after pre-ageing.

3.2. DSC studies

3.2.1. As-quenched state. Figure 3 summarises the heat flow curves obtained when the quenched alloys undergo continuous heating up to 550 °C; note again that the first 3 min are lost.

The behaviour of alloy 1 is comparable to that of an Al-2 mass% Cu-1.3 mass% Mg alloy investigated by Charaï *et al.* [20] and was interpreted as follows:

- formation of GPB zones (peak around 80 °C amounting to about -8.5 Jg^{-1}),

- dissolution of GPB zones (around 200 °C) and partial transformation into S″ (overlapping exothermic peak around 220 °C),

- S″ dissolution around 250 °C,

- precipitation of S′ (peak around 290 °C) partly overlapping with S″ dissolution, partial transformation of S′ into S (peak asymmetry)

- finally dissolution of S′ and S accompanied by a heat value of 17 Jg^{-1} before reaching the high temperature SS around 480 °C.

It was observed [20] that in quenched and RT aged alloys, S″ is formed during the DSC analysis from GPB zones, whereas, when aged at higher temperatures or longer times, it is formed preliminary to the DSC scan (hence the exothermic heat flows accompanying GPB zones $\rightarrow$ S″ transformation become increasingly smaller). The same interpretation is adopted for alloy 1, as the presence of the S″ phase is confirmed in the present study (§3.3).

[Insert fig. 3]

A heat balance shows that the decomposition of the SSSS starts immediately after quenching of alloy 1 and involves a heat loss of about 2 Jg^{-1} before DSC analysis. In alloys 2-5, such a heat loss is less noticeable. For alloy 5, heat values for GPB zone formation on one hand and S′ (S) formation or dissolution on the other hand are about 10 and 16 J/g respectively, with an uncertainty of ± 1 Jg^{-1}. GPB zone formation enthalpies obtained during heating at 20 $Kmin^{-1}$, when compared to values determined from isothermal calorimetry, are smaller; in fact, long-time isothermal ageing enables more important growth. On the contrary, S′ formation enthalpies obtained during

continuous heating are higher than values from isothermal calorimetry, as S″ dissolution overlaps much less. The most interesting result concerns the beginning of GPB zone formation: it is shifted to higher temperatures (i.e. retarded) when going from alloy 1 to alloys 5, 2 and 4. The GPB peak temperatures shift in the same order.

In the Ag-containing alloys 2 and 4, two small exothermic peaks appear at medium temperatures (around 250 and above 300 °C) instead of the strong and asymmetric one in alloys 1 and 5; they are separated by a very small endothermic peak. An increasing Ag content moves the exothermic effects to lower temperatures. The first peak is attributed to the formation of the X′ phase, since this phase was identified by electron microscopy in alloy 2 aged for 1 h at 240 °C [37]. The second exothermic peak is presumably associated with the precipitation of S′, as the peak temperature of alloy 4 is close to the S′ formation peak of the ternary alloy 1. In alloy 2, X′ precipitates later than in alloy 4 hence starts to dissolve later. The corresponding endothermic effects overlap more substantially the S′ exotherm whose peak temperature no longer corresponds to its highest precipitation rate.

The Si content in alloy 5 exceeds the solubility limit which approximates 0.1% at 520 °C according to Hutchinson and Ringer [22]; hence Mg_2Si precipitates are expected to be present after quench and their volume fraction should increase during ageing at 200 °C [22]. This may provoke the small exothermic effect observed around 180 °C which overlaps with GPB zone dissolution in figure 3, as well as the small dissolution effect before reaching the SS due to its increased solubility in this temperature range. Another interpretation would be that the three endotherms >145 °C correspond to the successive dissolution of zones typical for Al-Mg-Si alloys present in a small amount, GPB zones and the S″-phase.

3.2.2. Ageing at RT after quenching or reversion. Curves obtained after several months of ageing at RT are given in figure 4. GPB zone dissolution starts at increasingly higher temperatures when going from alloy 4 to 2, 5 and 1; this reflects greater zone sizes which necessitate higher reversion temperatures. The overlapping exothermic effects >130 °C and >150 °C well visible in the Ag-containing alloys 4 and 2, respectively, may be due to new zones precipitating during the DSC scan, such as in the case of alloy 1 aged for shorter times (figure 5).

If alloy 1 spends 3 h at RT before the DSC scan (figure 5, curve a), some GPB zones precipitate during the DSC scan from the still SSSS around 100 °C; they get partially dissolved during further heating but new zones appear for temperatures higher than 150 °C, as can be deduced from the overlapping exothermic peak. This peak is still visible after 7 h ageing (curve b) but absent after ageing for times ≥ 1day (curve c). This was attributed to the retention of excess vacancies enabling size evolution during heating [43]. When increasing the ageing time at RT after quenching, the S′ precipitation peak in the subsequent DSC scans become increasingly sharper; their start and peak temperatures are lower than after quenching (cf. curves a and c in figure 5 and curves 1 in figures 3 and 4).

[Insert figs. 4 and 5]

When most of the excess vacancies are eliminated by a 4 min hold at 230 °C after quenching, GPB zone formation is extremely slow at RT (no measurable heat flow in a calorimeter at 30 °C) but becomes visible for temperatures higher than 100 °C during a DSC run at 20 K/min (figure 5, curve d); the S′ formation peak starts a bit earlier than after water quenching and its heat value is not well reproducible, probably due to some initiation of S′ precipitation during short holding at 230 °C. RT ageing after reversion

has little influence on the shape and temperature position of the S′ peak (hence curves are not reproduced).

3.2.3. Ageing at 150 °C. Figures 6(a) and 6(b) display DSC curves obtained for alloy 1 and 2, respectively, aged for specified times at 150 °C before DSC analyses (note the different ordinate scale). It appears that a 10 min hold is sufficient to involve significant GPB zone formation (also observed for alloys 3, 4 and 5); their sizes (i.e. stability against heating) increase when passing from alloy 4 to 2, 5 and 1, just as after RT ageing. In alloy 1 (see figure 6(a)), the amount of S″ (endothermic peak around 255 °C) decreases after about 1 day in favour of S′ formation reflected by progressively decreasing S′ peaks during the subsequent DSC scans; this time corresponds to the second hardness rise [3,18]. The curve obtained after 3 months of ageing indicates that the phases S″, S′ and S co-exist; their dissolution enthalpy amounts to 25 J/g. Pre-ageing for 8 days at RT before 1 day ageing at 150 °C (curve PA) promotes the transformation of GPB zones into S″ (smaller GPB zone and earlier S″ dissolution peaks); it also leads to a much sharper S′ precipitation peak, hence to a narrower S′ size distribution than after direct ageing for 1 day at 150 °C.

[Insert figs. 6(a) and (b)]

Increasing the ageing time of alloy 2 at 150 °C from 1 h (start of second hardening stage according to Vietz and Polmear [3]) to 1 day increases the importance of the second endothermic peak in figure 6(b) which overlaps GPB zone dissolution and is attributed to S″ dissolution; the X′ formation peak around 250 °C becomes slightly reduced. Between 1 and 4 days, the amount of S″ decreases and that of X′ increases strongly; S′ appears as well (leading to a reduction of the X′ and S′ peaks during subsequent analyses). After 3 months ageing at 150 °C, the phases S″, X′ and S′ co-

exist. Pre-ageing at RT promotes X′ precipitation at 150 °C (smaller X′ peak during DSC analysis). In alloy 4, formation of X′ is even more advanced during the same time (not shown).

3.2.4. Ageing at 200 °C. Alloys 1, 2 and 5 were also aged at 200 °C for different times and examined by DSC (figures 7(a-c)). The curves indicate the presence of GPB zones after 2 min hold; a certain amount can still form during the scan from the still SSSS. Figure 7(a) shows that the amount of S″ in alloy 1 decreases progressively in favour of S′ precipitation at ageing times > 10 min; the latter phase is already present after 1 h hold at 200 °C when the hardness starts its second rise [3]. After 4 hours, the presence of GPB zones, S″ and S′ can be deduced from the subsequent DSC scan; these phases were actually detected besides clusters in a similar alloy [20]. Dissolution of S″, S′ and S co-existing after 1day needs about 25 J/g.

[Insert figs. 7(a),(b),(c)]

Alloy 5 shows a somewhat different behaviour (figure 7(b)). The second endothermic subpeak increases when prolonging the ageing time at 200 °C from 2 min to 1 hour; its maximum lies at 270 °C, temperature higher than for alloy 1. This may be indicative of the presence of an additional phase, probably θ″ or very small θ′. After 4 hours, the DSC curve shows a rather asymmetric precipitation peak. It is proposed that residual S′ formation is preceded by some θ′ precipitation, as can be observed on aged Al-4% Cu-0.3% Mg alloys [43]. Diffraction streaks attributed to monolayered GPB zones by Charaï *et al.* [20] were detected after ageing for 5 min and for 10 h (near peak hardness) at 200 °C [22,44]. After 15 h hold at 200 °C, a mixture of metastable phases co-exists and cannot be resolved by DSC (figure 7(b)). In principle, the temperature

span of the endothermic effects corresponds to the dissolution of big GPB zones, S″, θ″, θ′ (→θ) and S′ (→S) phases.

Curves obtained on the Ag-containing alloy 2 aged at 200 °C (figure 7(c)) confirm rapid X′ precipitation, as the DSC peak attributable to X′ formation is strongly reduced after 10 min. A new hardness rise was observed between 3-4 min [3]. At longer ageing times, DSC analyses start with S″ and X′ dissolution (see curves for 3 and 15 h). The DSC scan after 1 day ageing indicates X′, S′ and S dissolution.

3.3. Electron microscopy studies

As many observations were already done on the alloys studied (e.g. 15,22,37), only one heat treatment was examined in order to check the existence of the highly disputed S″ phase. Alloy 1 was quenched and aged at 180 °C for 15 h corresponding to the time position of the heat flow minimum in figure 2 (curve 1). Figures 8-10 display HRTEM images and their corresponding Fourier transforms. Clusters are mainly disordered according to figure 8 which shows no discrete diffraction spots.

The precipitate observed on figure 9 is identified as an S″/GPBII particle considering that its FFT is identical to those previously published by Charaï *et al.* [20] and Kovarik *et al.* [45]. Based on their HRTEM observations, two structures have been proposed recently for S″/GPII in alloys with Cu:Mg ratios >1 [27] and <1 [45]. Both are orthorhombic structures coherent with the fcc structure of the matrix but with somewhat different atom arrangements and compositions. Based on these structures, simulated HRTEM images and diffraction patterns along one particular orientation match the observed HRTEM and FFT images.

Figure 10 displays the HRTEM image and its FFT of an S′ precipitate, identical to those previously published [20].

[Insert figs. 8, 9 and 10]

4. Discussion

4.1. Formation of clusters and GPB zones.

In this paper, the question of GPB zone formation in an Al-2.5% Cu-1.5% Mg alloy without or with small Ag or Si additions has been re-examined using calorimetric measurements. Considering that the solid solutions are probably short-range ordered (see introduction), it can be expected that this tendency to clustering gets amplified upon quenching and that a metastable phase develops from clusters during ageing. According to figure 1, this phase precipitates at low ageing temperatures via a nucleation and growth controlled process and its heat value amounts to –13.5 J/g. Values of this order accompany the formation of Guinier-Preston zones in many Al-base alloys. In an Al-4% Cu alloy, for instance, formation of GP zones at RT (which contain 25-100 % Cu and whose identification by X-ray or electron diffraction does not constitute any problem) yields about –10 Jg^{-1} [46], hence the higher value for the ternary alloy containing less Cu can be explained by the decreased Cu solubility in the presence of Mg and the strong interaction between the Cu and Mg atoms. Therefore it seems reasonable to attribute this peak to the formation of GPB zones, although direct microscopic evidence for their existence in alloys 1–5 aged at temperatures < 150 °C is still lacking due to their extremely small sizes and lack of contrast. This proposition is also supported by Silcock [10] who observed X-ray diffraction effects in single crystals of a similar alloy, Al-3.1% Cu-1.5% Mg aged at RT, and attributed them to the presence of GPB zones. In Al-Mg alloys, GP zones only appear for Mg concentrations above about 10 % [47].

The proposed formation of GPB zones during low temperature ageing of Al-Cu-Mg alloys is in contradiction with recent conclusions of Starink *et al.* [25] drawn from 3D-AP analyses, calorimetric and hardness measurements. The authors propose that decomposition starts with Cu atom clustering and that Mg co-clustering is responsible for both the heat flow minimum and rapid hardening.

Following Ringer *et al.* [14,15], the cluster sizes observed at 150 °C correspond to entities of typically 10-50 atoms, hence they contain very few solute atoms. As their sizes at RT are even smaller and a high concentration of quenched-in vacancies provides rapid diffusion, formation of clusters is not expected to encounter nucleation difficulties reflected by a heat flow minimum. Moreover, it may be objected that the heat values measured on Al-Cu-Mg alloys are too high to correspond to the formation of clusters which contain only about 10 % solute atoms and many vacancies [23-25].

For the S″ phase (or GPBII), Wang and Starink [27] propose a solute concentration of 37.5%, which seems reasonable as the stable phase contains 50 % solute atoms.

4.2. Influence of Ag or Si additions

Small Ag additions ranging from 0.4 to 2 % (alloys 2-4) progressively reduce the rate of GPB zone formation, increasingly with the Ag content. An addition of 0.5 % Si (alloy 5) has a similar but less pronounced effect. These results agree with hardness measurements when comparing alloys 1 and 2 aged at 30 °C [18] or alloys 1 and 5 aged at RT [22].

A literature survey [48] yields the following binding energy values (in brackets) between vacancies and the following atoms: Cu (0.20 eV), Si (0.24 eV), Ag (0.27 eV) and Mg (0.33 eV). Hence Si and Ag atoms also trap vacancies and make the diffusion of Cu atoms increasingly difficult, thus leading to decreased zone sizes. Applying APFIM

to the Ag-bearing alloy 2 aged for 5 min at 150 °C, Ringer *et al.* [15] have detected

Mg-Ag co-clusters besides numerous Mg clusters and Mg-Cu co-clusters. They

consider that Mg-Ag clusters stimulate precipitation of the X′ phase. Figure 3 supports

that X′ forms the more rapidly the higher is the Ag concentration, hence the cluster

density and the vacancy concentration retained. Pre-ageing at RT does not strongly

influence X′ precipitation during DSC heating of alloys 2 and 4 (cf. figures 3 and 4) but

enhances X′ formation during isothermal ageing at medium temperatures (curve PA in

figure 6(b)). This may be due to bigger Mg-Ag clusters developed during pre-ageing,

which partly survive.

Several effects can be predicted for Si additions to Al-Cu-Mg alloys. Si atoms

may be present in Mg-rich and Si-rich clusters as well as in GPB zones; some zones

characteristic of Al-Mg-Si alloys may also appear. EDS spectra of Hutchinson and

Ringer [22] show that clusters called GPB zones contain Cu, Mg, Si and Al.

Furthermore, it has to be taken into account that only a small amount of Si (up to about

0.1%) is soluble at 520 °C in the present ternary alloy [22]; the excess Si is bound in the

form of Mg_2Si, hence it decreases the soluble Mg content and the as-quenched hardness

value. The alloy shifts progressively from the $(\alpha + S)$ into the $(\alpha + S + \theta)$ phase field, as

described by Hutchinson and Ringer [22]. Hence the precipitation behaviour will

depend on the Si content:

-        According to Smith *et al.* [38], a Si addition of 0.1 % slightly enhances S′

formation. Nucleation may be easier in the presence of soluble Si which interacts with

Mg and vacancies and decreases the shear strain energy [49] and the critical nucleus

size for S′ precipitation [50]. Smith *et al.* related the enhancement to earlier zone

dissolution which is indeed necessary before S′ precipitation and contradicts the

commonly accepted continuous sequence SSSS $\rightarrow$ GPB zones $\rightarrow$ S″ $\rightarrow$ S′ $\rightarrow$ S. The

present DSC curves indicate that direct transformation of GPB zones and S″ into S′ is of little significance at a heating rate of 20 Kmin[-1]. This also applies to binary Al-Cu alloys: during heating at 20 Kmin[-1], all GP zones dissolve before precipitation of θ′; at lower rates, however, reversion is only partial [51,52].

-        When the Si content exceeds the solubility limit, as in alloy 5, Mg_2Si particles are present after quenching and S′ formation is delayed with respect to the ternary alloy, especially after ageing at RT (figure 2). Slower S′ precipitation was also found in earlier DSC measurements [36] and in mechanical property and TEM studies of Wilson *et al.* [35]. They have attributed the observed refined size distribution of the S′ particles to a more homogeneous nucleation process related to the decreased density of dislocation loops and helices in the presence of Si. The present DSC curves indicate some S′ size refinement, the exothermic peak around 300 °C being sharper for alloy 5 than for alloy 1 (figure 3).

4.3. Influence of pre-ageing at RT on S′ precipitation

During continuous heating, the shape and temperature range of the main exothermic effects observed on alloy 1 change when RT ageing is carried out after quenching. The peaks become sharper indicating S′ size refinement; their initial, peak and end temperatures shift progressively to lower values with increasing ageing time (cf. curve 1 in figure 3, curves a, b and c in figure 5 and curve 1 in figure 4). On the contrary, pre-ageing at RT has no significant influence on S′ precipitation during heating of alloy 5 (cf. curves 5 in figure 3 and 4). This is also true in the case of a reverted alloy 1; samples aged after reversion have S′ peaks similar to those of curve 4 in figure 5.

The changes observed on alloy 1 can be explained by an easier homogeneous nucleation (the main process accompanied by heat flow minima in figure 2) resulting

from a higher density of clusters of overcritical size and/or by easier heterogeneous nucleation due to an increased defect density. In fact, the density and size of dislocation loops become higher when ageing alloy 1 at RT (Hutchinson and Ringer [22]), whereas loop formation is expected to be negligible after reversion due to vacancy loss at 230 °C. Growth of helices was observed in the Si-bearing alloy 5 during prolonged natural ageing but loops were not seen [22]. It seems that in a quenched ternary alloy, RT ageing favours mainly heterogeneous precipitation on dislocation loops, in agreement with Ber and Davydov [53]. Dislocations introduced by cold working in a quenched ternary alloy also strongly enhance S′ precipitation upon heating and assure a finer size distribution which improves the mechanical properties of the alloy [29].

4.4. First and second hardening stages

It was proposed by Charaï *et al.* [20] that in quenched Al-2%Cu-1.3%Mg alloys having a Mg:Cu atomic ratio of 1.6, GPB zones develop from very small Cu-rich clusters during the first minutes of ageing, whereas Mg-rich clusters containing excess vacancies absorb Cu atoms and become effective nuclei only at medium temperatures. In fact, the as-quenched hardness (AQ) values of Al-2.5% Cu alloys with Mg additions varying from 0.5 to 2%, are increasing with the Mg content, whereas the net hardness rise during the first hardening stage is similar except for the alloy containing only 0.5% Mg, hence with a Mg:Cu atomic ratio < 1 (Vietz and Polmear [3]). Also during the second stage of hardening in semi-logarithmic presentation, the net increase is rather independent of the Mg concentration in the range 150–200 °C, yet its onset is progressively delayed with increasing Mg content. In fact, Mg atoms are expected to inhibit Cu atom diffusion which seems to be the rate controlling step.

The important heat values measured on alloys lying in the (α + S) region of the ternary phase diagram depend primarily on the Cu content of the alloy. This supports the idea that GPB zones are responsible for the **first hardness stage.** The initial hardness increase at RT in an Al-4.4% Cu-1.7% Mg alloy has also been assigned to the formation of GP and GPB zones [54]. Clusters which contain much less solute atoms, are expected to contribute already to the AQ hardness level via the cluster hardening mechanism first proposed by Ringer *et al.* [15,26]. Other mechanisms may also be involved such as SS hardening, modulus hardening [25], dislocation loop hardening [17], solute atom - dislocation interactions [8] which favour subsequent heterogeneous nucleation of S′ and S.

The sizes of GPB zones (and probably of some Si-modified GPB zones in Si-bearing alloys) decrease when adding Si, and even more when adding Ag to the ternary alloy. This zone refinement may be mainly responsible for the fact that a higher net hardness increase at 150 °C (difference between value obtained after 2 min ageing and AQ value) is achieved when adding Ag (Vietz and Polmear [3]) than when adding Si [39], considering equivalent Cu and Mg concentrations in these alloys. It has also been shown [18] that the hardness of alloy 2 surpasses that of alloy 1 for long ageing times at 30 °C. At 200 °C, however, there is an exceptionally high increase when adding Si; it can be attributed to the formation of additional phases typical for Al-Cu alloys, namely θ'' via GP zones and θ', as alloy 5 lies at the border of the (α + θ + S) field of the phase diagram section at 190 °C [22]. In fact, GP zones were found in Al-1.5 %Cu-0.75 %Mg alloys containing >0.3 % Si [55]. The presence of θ' was observed by Gupta *et al.* [56] at 190 °C (>0.3 % Si); Hutchinson and Ringer [22] found θ and $\sigma(Al_5Cu_6Mg_2)$ in overaged alloy 5 ($\geq$20 h at 200 °C). Hence the asymmetry in the exothermic peaks in figure 2 (curve 5 at 180 °C) and figure 7(b) (4h at 200 °C) can be attributed to (further)

θ′ and S′ formation. The θ′ phase is expected to precipitate earlier than the S′ phase, as the less stable GP zones dissolve earlier [43].

A comparison of the hardness (Vietz and Polmear [3]) and DSC measurements (figures 6(a) and 7(a)) shows that during the **second hardness rise** at 150 °C (>1 day) and 200 °C (>1 h), the proportion of GPB zones and S″ diminishes and that of S′ increases in the ternary alloy. Hence this stage can be related to fine S′ particles which precipitate probably at the sites of clusters, as shown by HRTEM [22,30]. The necessary Cu atoms are provided by the progressive dissolution of less stable phases and the decreased solute solubility in the presence of more stable phases, which increases the fraction precipitated and the corresponding heat value.

In the Ag containing alloys 2-4, the second hardening stage sets in rapidly at medium temperatures. According to hardness measurements on alloy 2 aged at 150 °C, its start falls between 1 h [3] and 10 h [57]; these largely varying times may be due to difficult subjective appreciation and different experimental conditions. DSC scans indicate already S″ and X′ formation in this time range (figure 6(b)). The precipitation of X′ continues between 1 and 4 days, whereas GPB zones and S″ dissolve progressively and some S′ appears. Hence the second hardness rise may be attributed mainly to the precipitation of the X′ phase, as proposed by Ringer *et al.* [15], and supports the proposition of its initial coherency with the matrix. At peak hardness reached between 5 [3] and 20 days, X′ is probably semi-coherent (Ferragut *et al.* [57]).

When alloy 2 is aged at 200 °C, a second hardness rise becomes observable in semi-logarithmic presentation after 3-4 min [3]. According to figure 7(c), there is notable precipitation of the X′ phase between 2 and 10 min, S″ being also present and dissolving in favour of S′ at longer ageing times. At maximum hardness (about 3 h), the

phases S″, X′ and S′ co-exist, as a subsequent DSC scan starts with S″ and X′ dissolution before precipitation of residual S′.

5. Conclusions

Calorimetric measurements at constant temperatures and during heating at 20 K.min^{-1} provided the following information about the effects of 0.4 to 2% Ag or 0.5% Si additions to an Al-2.5 mass% Cu-1.5 mass% Mg alloy:

1   The precipitation of GPB zones obeys a well visible nucleation and growth controlled process at low temperatures; its rate is reduced with respect to the ternary alloy due to the vacancy-trapping effect of soluble Si and, even more, of Ag atoms. This results in zone refinement and hardness increases.

2   A Si addition of 0.5% induces θ′ prior to S′ precipitation at medium temperatures.

3   In the Ag-containing alloys, an additional phase, X′, appears before S′. It forms earlier when the Ag addition (hence the density of Mg-Ag clusters) is increased.

4   Pre-ageing at RT enhances S′ formation in the ternary alloy and causes a narrower size distribution; in an alloy containing 0.5% Si, it retards isothermal θ′ and S′ formation; in the Ag-containing alloys, it promotes isothermal X′ formation.

5   Correspondence between DSC curves and existing hardness data support the original interpretation, i.e. the first hardening stage results from the formation of GPB zones which transform into the S″ phase (the existence of which was again proven by HRTEM). During the second hardening stage in logarithmic time scale, S′ particles nucleate after incomplete reversion of GPB zones and S″, and increase the volume fraction precipitated.

6   In the Ag-containing alloys, the second hardening stage sets in much earlier than in the ternary alloy and is related mainly to the precipitation of X′.

7   The very high hardness increases in the Si-containing alloy can be attributed to the

formation of additional phases typical for binary Al-Cu alloys.

References

[1] G.B. Brook, *Precipitation in Metals*, Special Report n° 3 (Fulmer Research Institute, Stoke Poges, UK, 1963).

[2] H.K. Hardy, J. Inst. Met. **83** 17 (1954-55).

[3] J.T. Vietz and I.J. Polmear, J. Inst. Met. **94** 410 (1966).

[4] P. Vigier, A.-M. Zahra-Kubik, M. Denoux, J.P. Brisset and M. Wintenberger, Mém. Sci. Rev. Mét. **69** 51 (1972).

[5] E. Matsubara and J.B. Cohen, Acta metall. **31** 2129 (1983).

[6] P. Chartrand and A.D. Pelton, J. Phase Equil. **15** 591 (1994).

[7] B.-P. Huang and Z.-Q. Zheng, Acta mater. **46** 4381 (1998).

[8] L. Reich, S.P. Ringer, and K. Hono, Phil. Mag. Lett. **79** 639 (1999).

[9] S. Hirosawa, T. Sato, A. Kamio and H.M. Flower, Acta mater. **48** 1797 (2000).

[10] J.M. Silcock, J. Inst. Met. **89** 203 (1960-61).

[11] A.-M. Zahra and C.Y. Zahra, Phil. Mag. Lett. **82** 9 (2002).

[12] B. Verlinden and A.-M. Zahra, Mater. Sci. Forum **426-432** 423 (2003).

[13] S.P. Ringer, K. Hono, I.J. Polmear and T. Sakurai, Appl. Surf. Sci. **94-95** 253 (1996).

[14] S.P. Ringer, K. Hono, T. Sakurai and I.J. Polmear, Scripta mater. **36** 517 (1997).

[15] S.P. Ringer, T. Sakurai and I.J. Polmear, Acta mater. **45** 3731 (1997).

[16] K. Raviprasad, C.R. Hutchinson, T. Sakurai and S.P. Ringer, Acta mater. **51** 5037 (2003).

[17] S. Kumai, M. Okutsu, N. Yoneyama and T. Sato, J. Jpn. Inst. Light Met. **52** 465 (2002).

[18] I.J. Polmear, Trans. Metall. Soc. AIME **230** 1331 (1964).

[19] M.J. Starink and A.-M. Zahra, Thermochim. Acta **298** 179 (1997).

[20] A. Charaï, T. Walther, C. Alfonso, A.-M. Zahra and C.Y. Zahra, Acta mater. **48** 2751 (2000).

[21] Y.A. Bagaryatskii, Dokl. Akad. NAUK SSSR **87** 559 (1952).

[22] C.R. Hutchinson and S.P. Ringer, Metall. Mater. Trans. **31A** 2721 (2000).

[23]   N. Gao, L. Davin, S. Wang, A. Cerezo and M.J. Starink, Mater. Sci. Forum **396-402** 923 (2002).

[24]   A.-M. Zahra, C.Y. Zahra, C. Alfonso and A. Charaï, Scripta Mater. **39** 1553 (1998).

[25] M.J. Starink, N. Gao, L. Davin, J. Yan and A. Cerezo, Phil.Mag. **85** 1395 (2005).

[26] S.P. Ringer, S.K. Caraher and I.J. Polmear, Scripta mater. **39** 1559 (1998).

[27] S.C. Wang and M.J. Starink, Mater. Sci. Eng. **A386** 156 (2004).

[28] H.-C. Shih, N.-J. Ho and J.C. Huang, Metall. Mater.Trans. **27A** 2479 (1996).

[29] A.-M. Zahra and C.Y. Zahra, J. Therm. Anal. **36** 1465 (1990).

[30] V. Radmilovic, G. Thomas, G.J. Shiflet and E.A. Starke, Scripta metall. **23** 1141 (1989).

[31] G. Riontino and A. Zanada, Mater. Lett. **37** 241 (1998).

[32]   V. Radmilovic, R. Kilaas, U. Dahmen and G.J. Shiflet, Acta mater. **47** 3987 (1999).

[33] C. Wolverton, Acta mater. **49** 3129 (2001).

[34] L.F. Mondolfo, 1976, *Aluminium Alloys : Structure and Properties* (Butterworths, London, 1976).

[35] R.N. Wilson, D.M. Moore and P.J.E. Forsythe, J. Inst. Met. **95** 177 (1967).

[36] H. Kee Cho and K. Hirano, paper presented at the 5th Internat. Conf. Therm. Anal., Kyoto, Japan (1977).

[37] H.D. Chopra, L.J. Liu, B.C. Muddle and I.J. Polmear, Phil. Mag. Lett. **71** 319 (1995).

[38] G.W. Smith, W.J. Baxter and R.K. Mishra, J. Mater. Sci. **35** 3871 (2000).

[39] S.P. Ringer, I.J. Polmear and T. Sakurai, Mater. Sci. Eng. **A217-218** 273 (1996).

[40] L. Reich, K. Süvegh, J. Lendvai and A. Vertes, Phil. Mag. Lett. **81** 145 (2000).

[41] A.-M. Zahra and M. Laffitte, Scripta metall. **8** 165 (1974).

[42] C.Y. Zahra and A.-M. Zahra, Thermochim. Acta **276** 161 (1996).

[43] A.-M. Zahra, C.Y. Zahra, K. Raviprasad and I.J. Polmear, Phil. Mag. **84** 2521 (2004).

[44] C.R. Hutchinson, K. Raviprasad and S.P. Ringer, in *Proc. Internat. Conf. Solid-Solid Phase Transformations '99 (JIMIC-3)*, edited by M. Koiwa, K. Otsuka and T. Miyazaki (Jpn. Inst. Met., 1999), p. 169.

[45] L. Kovarik, P.I. Gouma, C. Kisielowski, S.A. Court and M.J. Mills, Acta Mater. **52** 2509 (2004).

[46] A. Zahra, M. Laffitte, P. Vigier and M. Wintenberger, Mém. Sci. Rev. Mét. **74** 561 (1977).

[47] M.J. Starink and A.-M. Zahra, Phil. Mag. **A76** 701 (1997).

[48] H. Löffler, *Structure and Structure Development of Al-Zn Alloys* (Akademie-Verlag, Berlin, Germany, 1995), p. 56.

[49] J.F. Nie, H.I. Aronson and B.C. Muddle, in *Proc. Internat. Conf. Solid-Solid Phase Transformations '99 (JIMIC-3)*, edited by M. Koiwa, K. Otsuka and T. Miyazaki (Jpn. Inst. Met., 1999), p. 157.

[50] F. Soisson and G. Martin, Phys. Rev. **B62** 203 (2000).

[51] A.-M. Zahra, M. Laffitte, P. Vigier and M. Wintenberger, C. R. Acad. Sci. **C277** 923 (1973).

[52]   A. Zahra-Kubik, M. Laffitte, P. Vigier and M. Wintenberger, Aluminium, **52** 357 (1976).

[53]   L.B. Ber and V.G. Davydov, Mater. Sci. Forum **396-402** 983 (2002).

[54]   S. Abis, M. Massazza, P. Mengucci and G. Riontino, Scripta mater.**45** 685 (2001).

[55]   A.K. Jena, A.K. Gupta and M.C. Chaturvedi, Metall. Trans. **24A** 2181 (1993).

[56]   A.K. Gupta, M.C. Chaturvedi and A.K. Jena, Mater. Sci. Technol. **5** 52 (1989).

[57]   R. Ferragut, A. Somoza, A. Dupasquier and I.J. Polmear, Mater. Sci. Forum **396-402** 777 (2002).

Figure Captions

Fig. 1: Isothermal calorimetry: heat flows of pure aluminium and of alloys 1, 2, 3 and 5 aged in the calorimeter at 30 °C.

Fig. 2: Isothermal calorimetry: heat flows recorded during ageing at 180 °C on alloy 1 after water quenching (curve 1), followed by ageing for 7 days at RT (curve 1a), or 4 days at 100°C (1b) and on alloy 5 after water quenching (curve 5) and followed by ageing for 7 days at RT (curve 5a).

Fig. 3: DSC at 20Kmin^{-1} on alloys 1, 2, 4 and 5 after water quenching.

Fig. 4: DSC at 20Kmin^{-1} on alloys 1, 2, 4 and 5 after water quenching and long room temperature ageing (9 months for alloys 1, 2, 4 and 14 months for alloy 5).

Fig. 5: DSC at 20Kmin^{-1} on alloy 1 after water quenching and ageing at RT for 3 hours (a), 7 hours (b), 1 day (c) or after water quenching and ageing for 4 minutes at 230°C (d).

Fig. 6: DSC at 20Kmin^{-1} on alloy 1 (a) and alloy 2 (b) after water quenching and ageing at 150 °C for times indicated on the figures. The response of samples pre-aged at RT (8 days for alloy 1, 2 months for alloy 2) after water quenching and aged at 150 °C for 1 day is also displayed (curves PA).

Fig. 7: DSC at 20Kmin^{-1} on alloy 1 (a), alloy 5 (b) and alloy 2 (c) after water quenching and ageing at 200 °C for times indicated on the figures.

Fig. 8: HRTEM image (a) and its Fourier transform (b) of a cluster observed in alloy 1 after water quenching and ageing for 15h at 180°C.

Fig. 9: HRTEM image (a) and its Fourier transform (b) confirming the presence of the S″ phase in alloy 1 after water quenching and ageing for 15h at 180°C.

Fig. 10: HRTEM image (a) and its Fourier transform (b) of a precipitate of the S′ phase observed in alloy 1 after water quenching and ageing for 15h at 180°C.
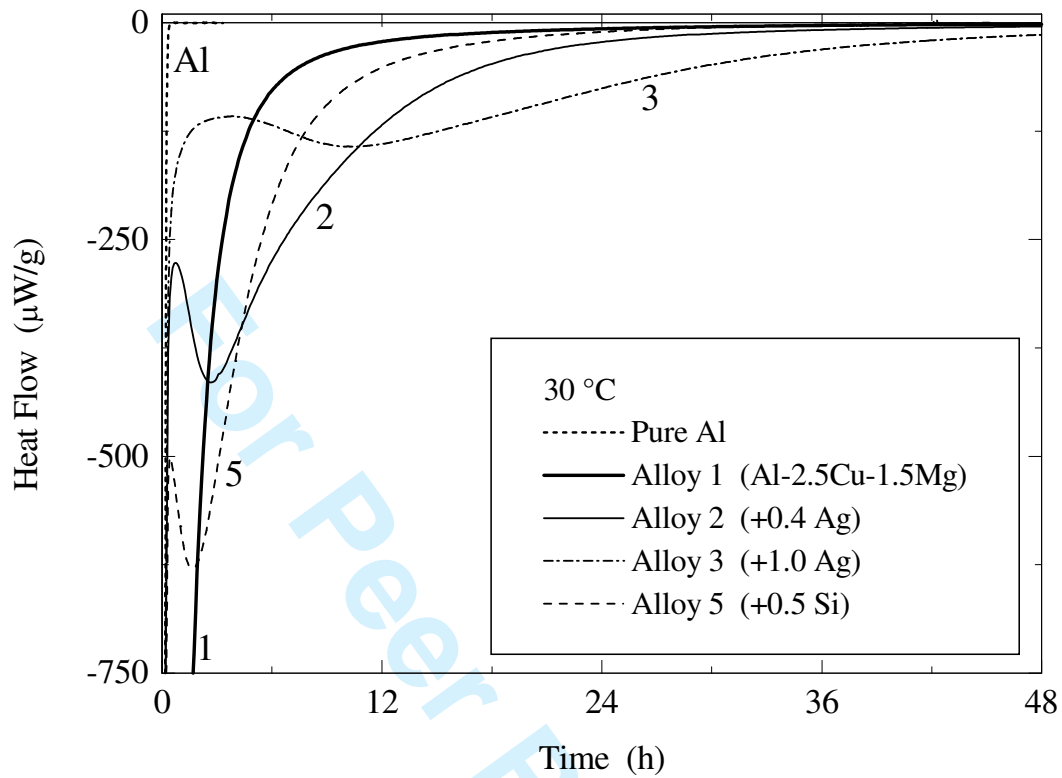
Figure 1: Isothermal calorimetry: heat flows of pure aluminium and of alloys 1, 2, 3 and 5 aged in the calorimeter at 30 °C.
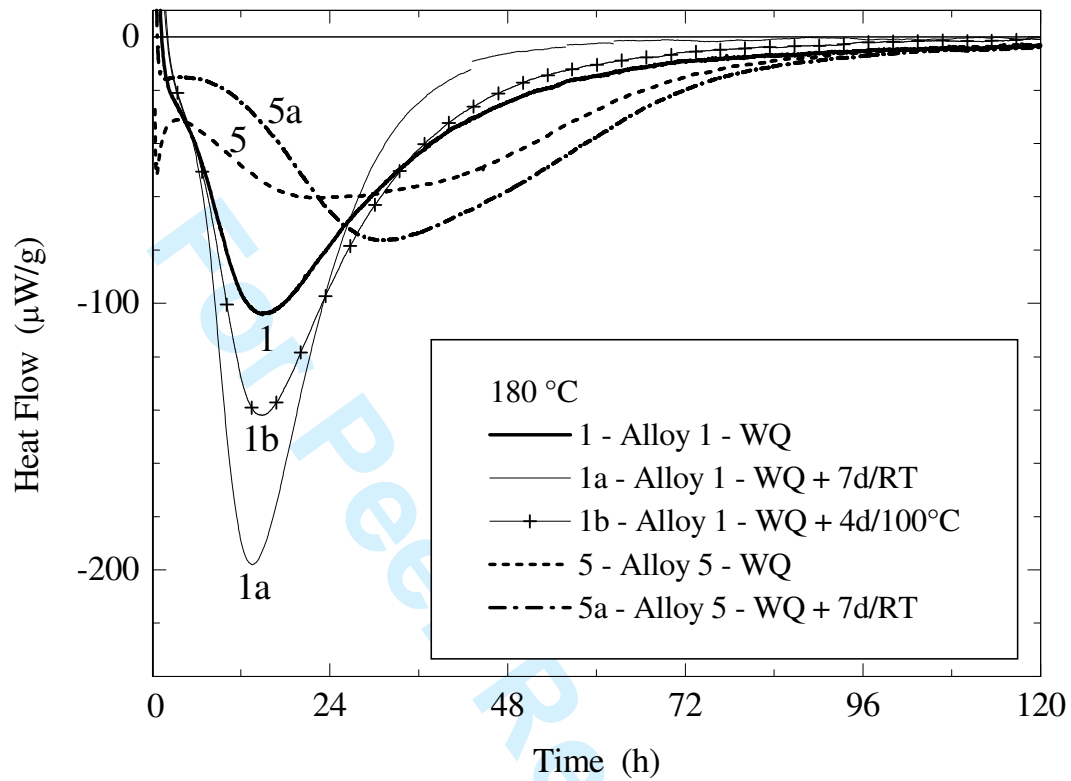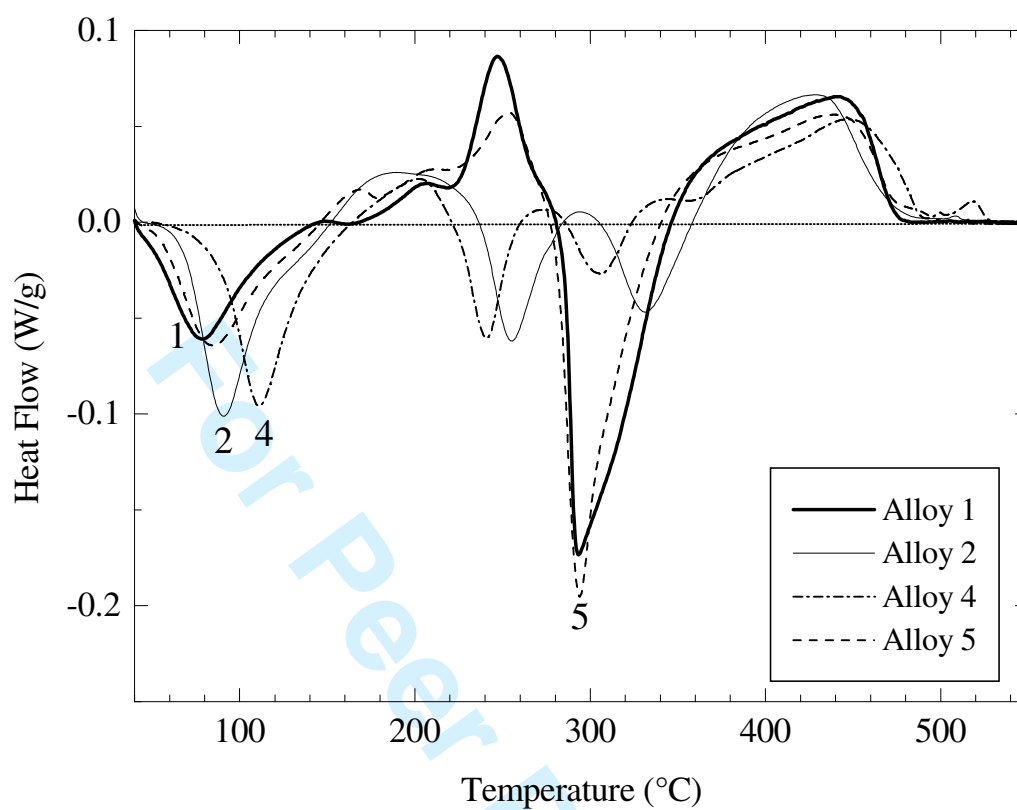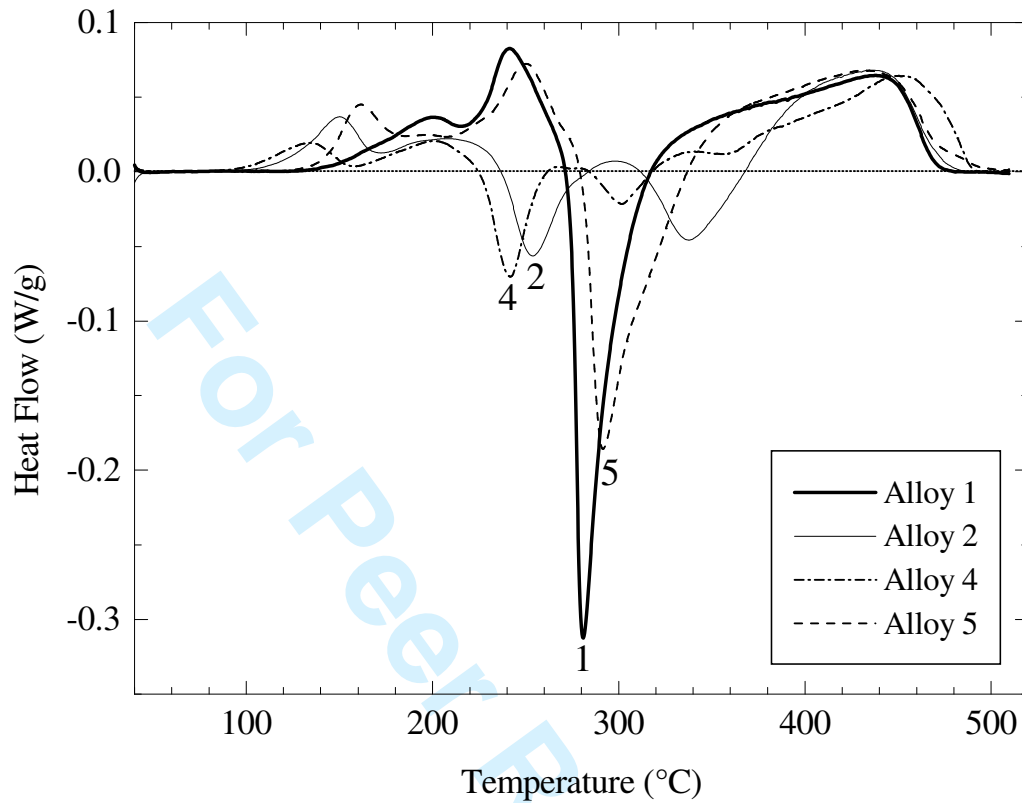
Figure 2: Isothermal calorimetry: heat flows recorded during ageing at 180 °C on alloy 1 after water quenching (curve 1), followed by ageing for 7 days at RT (curve 1a), or 4 days at 100°C (1b) and on alloy 5 after water quenching (curve 5) and followed by ageing for 7 days at RT (curve 5a).

Figure 3: DSC at 20Kmin^{-1} on alloys 1, 2, 4 and 5 after water quenching.

Figure 4: DSC at 20Kmin^{-1} on alloys 1, 2, 4 and 5 after water quenching and long room temperature ageing (9 months for alloys 1, 2, 4 and 14 months for alloy 5).
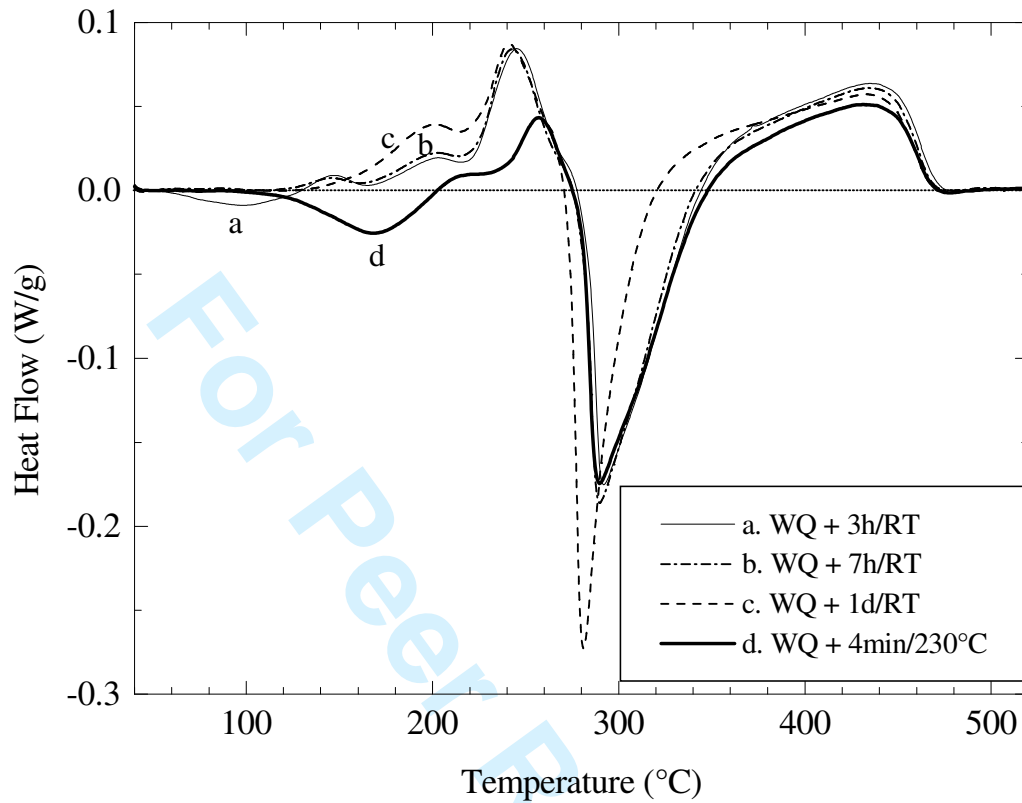
Figure 5: DSC at 20Kmin^{-1} on alloy 1 after water quenching and ageing at RT for 3 hours (a), 7 hours (b), 1 day (c) or after water quenching and ageing for 4 minutes at 230°C (d).
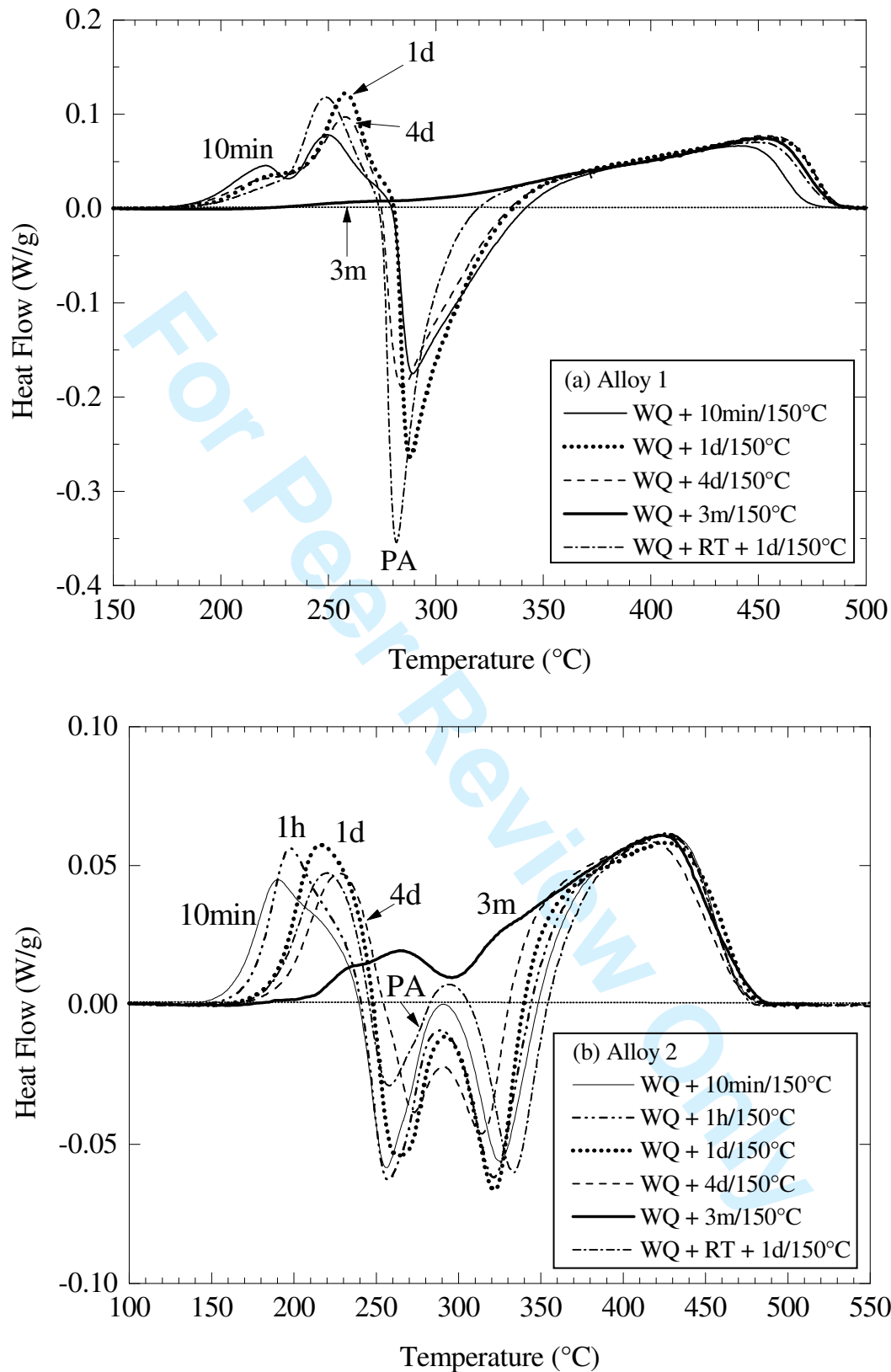
Figure 6: DSC at 20Kmin^{-1} on alloy 1 (a) and alloy 2 (b) after water quenching and ageing at 150 °C for times indicated on the figures. The response of samples pre-aged at RT (8 days for alloy 1, 2 months for alloy 2) after water quenching and aged at 150 °C for 1 day is also displayed (curves PA).
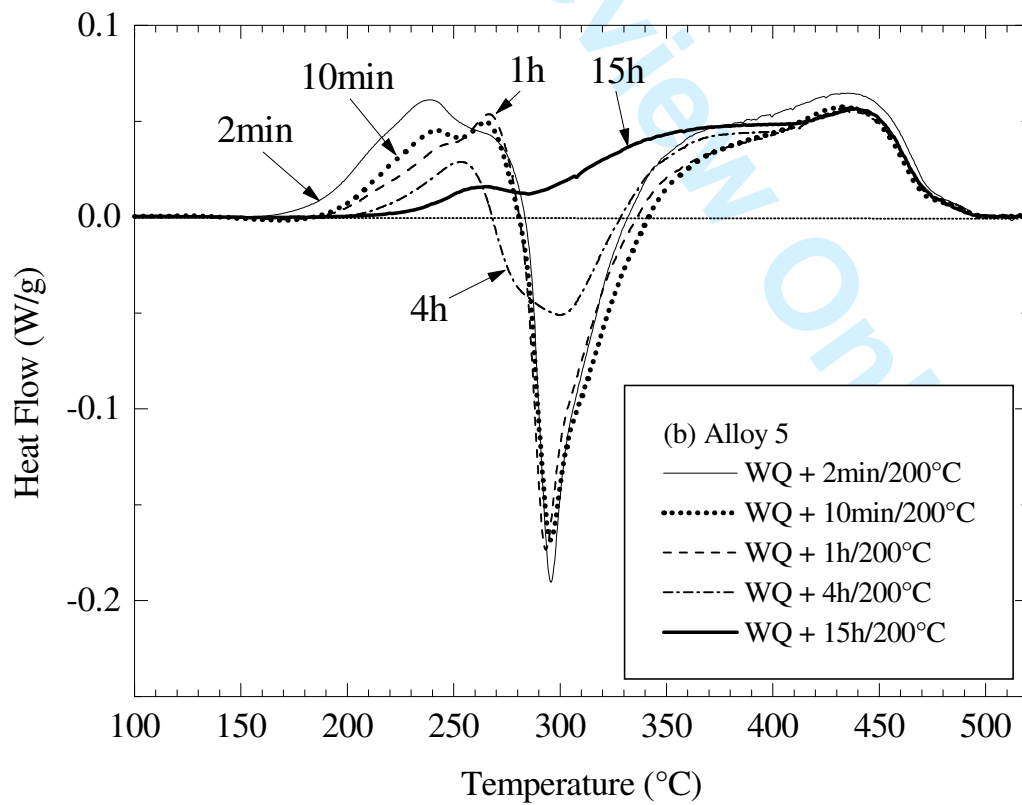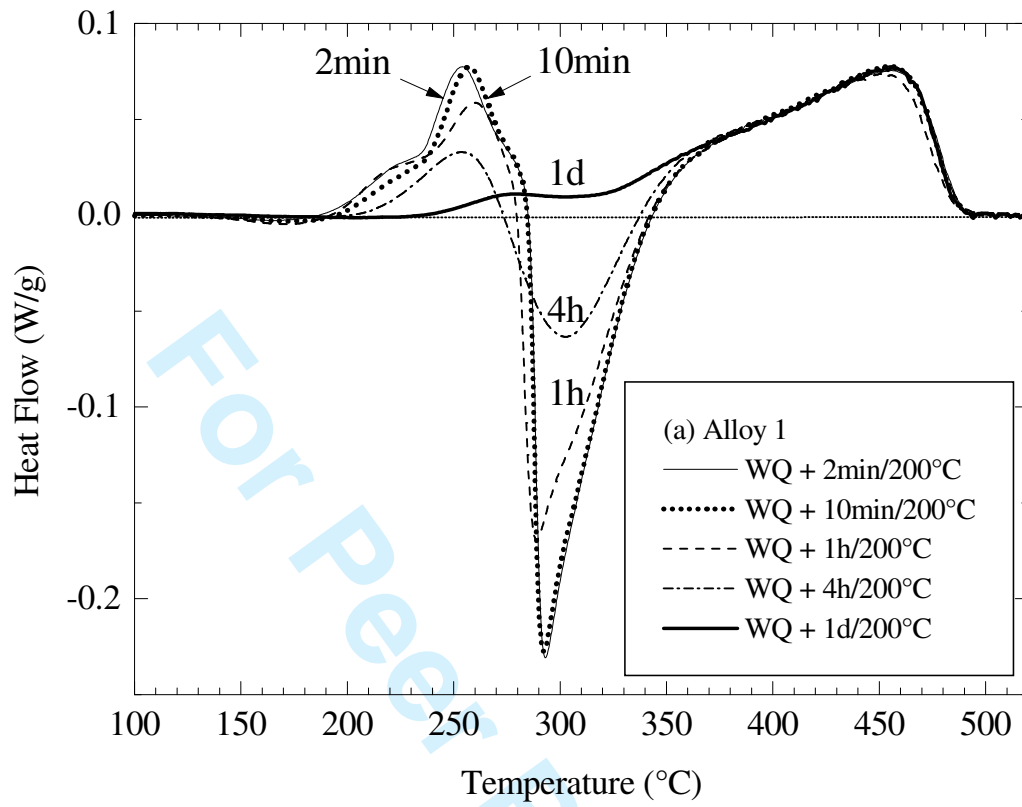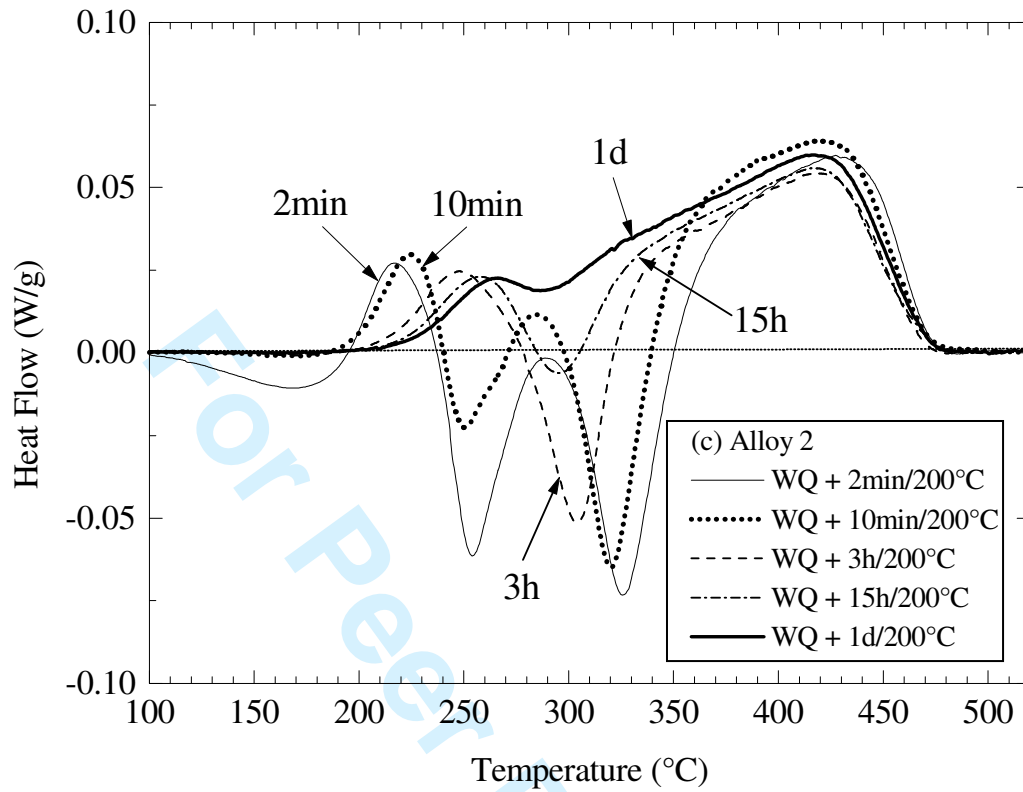
Figure 7: DSC at 20Kmin^{-1} on alloy 1 (a), alloy 5 (b) and alloy 2 (c) after water quenching and ageing at 200 °C for times indicated on the figures.
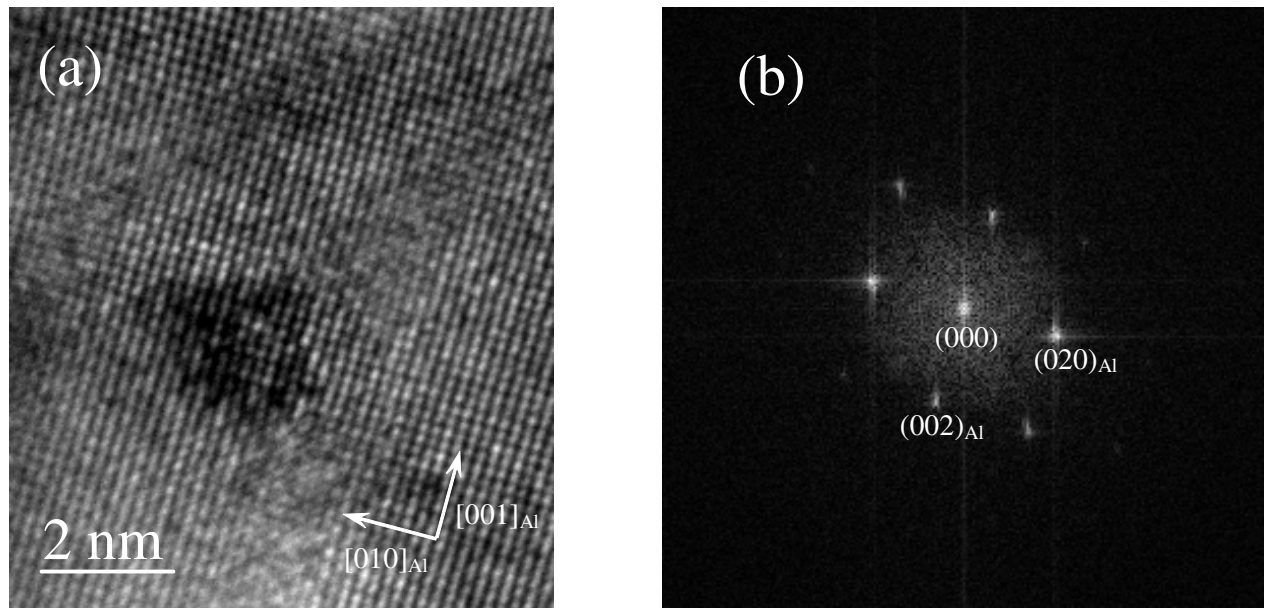
Figure 8: HRTEM image (a) and its Fourier transform (b) of a cluster observed in alloy 1 after water quenching and ageing for 15h at 180°C.
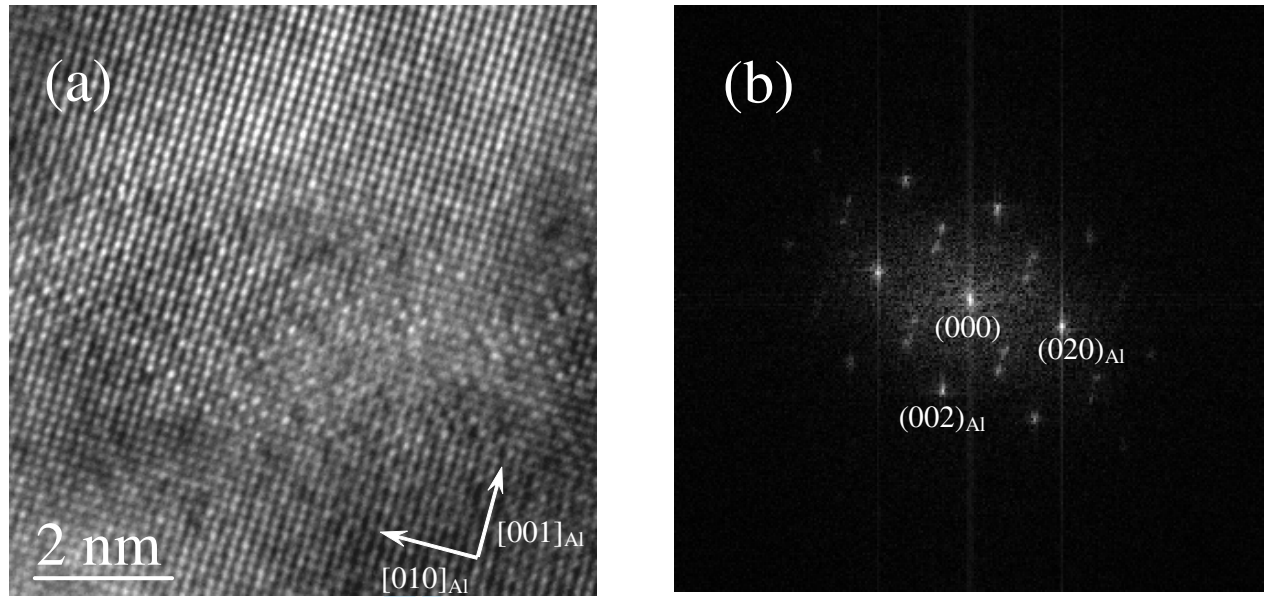
Figure 9: HRTEM image (a) and its Fourier transform (b) confirming the presence of the S″ phase in alloy 1 after water quenching and ageing for 15h at 180°C.
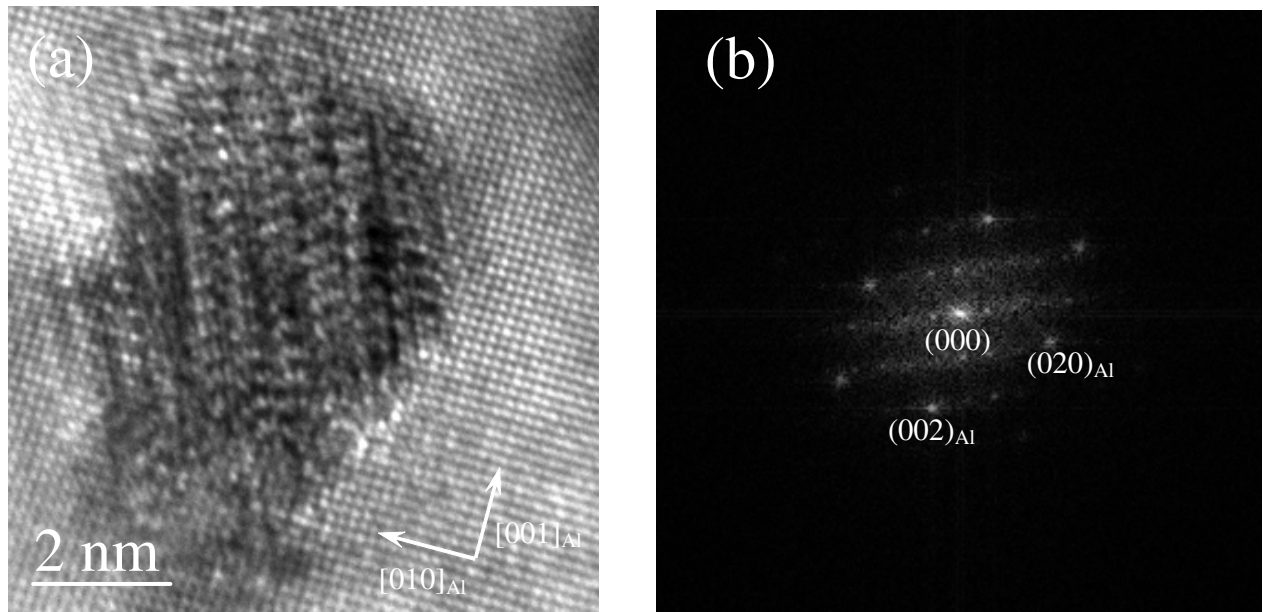
Figure 10: HRTEM image (a) and its Fourier transform (b) of a precipitate of the S′ phase
observed in alloy 1 after water quenching and ageing for 15h at 180°C.